

# Calculation of Friction in Steady-State and Transient EHL Simulations

C.E. Goodyer<sup>a</sup>, R. Fairlie<sup>a</sup>, D.E. Hart<sup>a</sup>, M. Berzins<sup>a</sup> and L.E. Scales<sup>b\*</sup>

<sup>a</sup>Computational PDEs Unit, School of Computing, University of Leeds, Leeds, LS2 9JT, United Kingdom

<sup>b</sup>Shell Global Solutions, Thornton, Chester, CH1 3SH, United Kingdom

The total friction through a lubricated contact is a physical quantity which may be measured experimentally in an EHL test rig. Numerical EHL simulations will wish to accurately reproduce the results from directly comparable simulations, and hence the friction will be one of the key variables of interest. It is shown that not only are very smooth meshes needed to resolve some features of EHL calculations but also that the accuracy achieved on standard quantities of interest such as minimum film thickness varies greatly and may not correlate well to quantities such as friction. The use of adaptive mesh techniques for steady problems is considered in the same context with results presented for how well the accuracy of the friction is maintained. This is generalised to transient cases with surface roughness, hence incorporating numerous pressure spikes needing accurate resolution.

## 1. INTRODUCTION

Solution times for numerical models of elastohydrodynamic lubrication (EHL) problems continue to decrease as the algorithms used improve and the computers on which they are solved become more powerful. Conversely as the lubricant models used by industry become more complex, the demands for robustness, accuracy and speed of the software increase. In addition as the breadth of cases increases the generality of the software must also increase, so a single code must be able to tackle a wide range of problems with the minimum of user input.

The broad requirements of a user of such a code is to obtain the “correct” solution as quickly as possible. This leads to the consideration of the question of what is meant by “correct”. In order to consider a solution “correct” it must satisfy some objective criteria and it may well be that the level of accuracy required to meet this criteria for one solution component is inadequate for another. Typically a finer resolution of computational mesh (grid) leads to more accuracy but at the expense of increased solution times. Therefore if the user is only concerned with solution components that already meet the objective “correctness” criteria at a certain level of grid resolution, it may be unnecessary

to increase the grid resolution further. However care must be taken as not only can solution components which are not accurately resolved affect other components, but in transient problems the growth of errors in these other components can result in completely inaccurate solutions. In this paper we study how to take these requirements into account when considering quantities such as friction.

In order to measure the error in a computational experiment it is necessary to measure how far the computational result is from the true solution. Since EHL problems only have an analytic solution in very special cases we will consider the “true” solution to be that obtained as the number of points increases, and hence the mesh spacing decreases. In particular, the “true” solution will be defined here by that computed on a very fine mesh, often termed a “truth mesh” in the computational science community. Providing the truth mesh is sufficiently fine, then it is possible to model the discretisation error on much coarser meshes.

Furthermore when comparing numerical results against experimental results the accuracy of the experiments themselves must be included for establishing the overall demands from the simulation.

In this paper we shall only concern ourselves with consideration of key variables, such as friction or central and minimum film thicknesses. The reasons behind this motivation are that in many real simulations

---

\*The authors would like to thank EPSRC, the DTI e-Science Core programme and Shell Global Solutions for funding this work. We also would like to thank the referee for useful comments improving the clarity of this paper.

being performed, these are likely to be the variables considered by the user [9]. We discuss the need for both high level and low level strategies for assessing the quality of the results. Use of techniques previously presented such as variable timestepping [11] and grid adaptation [10] are explained in the context of improved accuracy of solutions without jeopardizing the fast solution times.

Investigations into friction have been mainly confined to experimental work such as Blencoe *et al.* [4] and Workel *et al.* [22]. As will be shown in Section 4 the friction is related very closely to accurately capturing the profile of the pressure spike. Work by Bisset and Glander [2] showed that when more fine mesh points are used in the region of the spike then it is no longer seen as a singularity in the solution, but a smooth profile. This work did only resolve the spike using up to 1000 points, however it did still highlight the importance of this area of the solution. Further consideration of this area in respect to the elastic properties is given by Hall [13] and the benefits of this approach for better accuracy is shown by Lee and Hsu [15].

The consideration of friction will be seen to have great dependence on the resolution of the gradients in the pressure solutions, as will be explained with reference to the governing equations. The consideration of the resolution of the single pressure spike in a line contact case will be used as an example which must be applied to the much more general cases of surface roughness where sharp pressure spikes will occur through the length of the contact region. Accurate resolution of these gradients will lead to more reliable computational results for the key quantities of interest.

The rest of the paper is laid out as follows. In Section 3 the equations used in the solver are listed in non-dimensional form, along with a brief discussion of the solution methods used. The need for monitoring of key variables is outlined in Section 4 where increasing grid resolution is shown to make noticeable changes to solution profiles, particularly with reference to capturing the true gradients in the pressure solution. This work also shows the need for larger inlet regions in the computational domain. These ideas naturally feed into the use of grid adaptation for EHL problems. Techniques for doing this have been presented previously, e.g. [16,10], and in Section 5 it is shown how the use of multigrid patches for line contact EHL solutions can maintain very high accuracy

for the friction without requiring fine meshes over most of the domain. Transient problems involving surface roughness are considered in Section 6 where the resolution of the mesh is seen to dramatically affect the accuracy of the calculated friction. The paper is concluded in Section 7, with some suggestions for future work being made.

## 2. NOTATION

|                     |                                                     |
|---------------------|-----------------------------------------------------|
| $a$                 | half-width of Hertzian contact                      |
| $\mathcal{C}(A,B)$  | Correlation between $A$ and $B$                     |
| $\mathcal{F}$       | total friction through the contact                  |
| $G$                 | undeformed surface geometry                         |
| $H$                 | non-dimensionalised film thickness                  |
| $H_{00}$            | film thickness central offset                       |
| $k$                 | grid level in multigrid scheme                      |
| $p_h$               | maximum Hertzian pressure                           |
| $P$                 | non-dimensionalised pressure                        |
| $R_x$               | reduced radius of curvature                         |
| $T$                 | non-dimensionalised time                            |
| $u_s$               | sum of velocities of contacts                       |
| $U_1, U_2$          | non-dimensional rolling speeds of surfaces 1 and 2  |
| $X$                 | dimensionless coordinate                            |
| $X_l$               | dimensionless left boundary of computational domain |
| $Y$                 | dimensionless coordinate                            |
| $z$                 | viscosity index                                     |
| $\alpha$            | pressure viscosity index                            |
| $\varepsilon$       | coefficient in Reynolds equation                    |
| $\eta_0$            | viscosity at ambient pressure                       |
| $\bar{\eta}$        | non-dimensionalised viscosity                       |
| $\lambda$           | coefficient in Reynolds equation                    |
| $\mu_{11}$          | Covariance                                          |
| $\rho$              | convergence test parameter                          |
| $\rho_0$            | density at ambient pressure                         |
| $\bar{\rho}$        | non-dimensionalised density                         |
| $\sigma_A$          | Variance of $A$                                     |
| $\bar{\tau}_{xz,1}$ | non-dimensional shear stress on surface 1           |

## 3. EQUATIONS AND STANDARD SOLUTION METHOD

The equations governing EHL line contacts are given, in non-dimensional form, by the following set of three equations. Firstly, the pressure distribution is defined by the discrete form of the Reynolds Equation:

$$\frac{\partial}{\partial X} \left( \varepsilon \frac{\partial P}{\partial X} \right) - \frac{u_s}{u_s(0)} \frac{\partial (\bar{\rho} H)}{\partial X} - \frac{\partial (\bar{\rho} H)}{\partial T} = 0 \quad (1)$$

where  $\varepsilon$  and  $\lambda$  are given by

$$\varepsilon = \frac{\bar{\rho} H^3}{\bar{\eta} \lambda u_s(0)}, \quad (2)$$

and

$$\lambda = \frac{6 \eta_0 R_x^2}{a^3 p_h}. \quad (3)$$

The film thickness equation for line contact cases,

$$H(X, Y) = H_{00} + G(X, Y) - \frac{1}{\pi} \int_{-\infty}^{\infty} \ln |X - X'| P(X') dX', \quad (4)$$

defines the contact shape, for given undeformed geometry  $G(X, Y)$ .

The force balance equation,

$$\int_{-\infty}^{\infty} P(X) dX = \frac{\pi}{2}, \quad (5)$$

is also solved to provide conservation of applied force.

Unless otherwise stated, the lubricant model used is that of a generalised Newtonian fluid. The model used for viscosity is derived from the Roelands equation [17],

$$\bar{\eta}(P) = \exp \left\{ \frac{\alpha p_0}{z} \left[ -1 + \left( 1 + \frac{P p_h}{p_0} \right)^z \right] \right\}, \quad (6)$$

and for density an extended version of the Dowson and Higginson relation [6],

$$\bar{\rho}(P) = \left( 1 + \frac{5.8 \times 10^{-10} P p_h}{1 + 1.7 \times 10^{-9} P p_h} \right). \quad (7)$$

is used, as described in [7].

These equations are discretised on a regular mesh of  $(2^k+1)$  points. Both first and second order finite differences have been used. These have then

been solved using the multigrid techniques described in [20,21,8,7] and the multilevel multi-integration algorithm of Brandt and Lubrecht [5].

Once solutions for these equations are found it is possible to derive the shear stress on each surface [18]. These forces are defined to be

$$\bar{\tau}_{xz;1}(x) = -\frac{a p_h H}{2R} \frac{\partial P}{\partial X} + \frac{R}{a^2 \eta_0} \frac{\bar{\eta}}{H} (U_2 - U_1) \quad (8)$$

$$\bar{\tau}_{xz;2}(x) = \frac{a p_h H}{2R} \frac{\partial P}{\partial X} + \frac{R}{a^2 \eta_0} \frac{\bar{\eta}}{H} (U_2 - U_1) \quad (9)$$

for surfaces 1 and 2 at  $z = 0$  and  $z = H$  respectively moving at dimensionless speeds  $U_1$  and  $U_2$  respectively. From these expressions it is possible to work out the total (dimensional) friction through a line contact,  $\mathcal{F}$  as:

$$\mathcal{F} = \int_{-\infty}^{\infty} p_h \bar{\tau}_{xz;1}(x) dx. \quad (10)$$

This is a key quantity of interest as it can give a measure of the force opposing the shear in the lubricant, e.g. [3, Chapter 6]. The total friction is made up of the rolling friction and the kinetic friction, although experimentally these cannot be measured independently and hence in this work only the total friction will be considered.

#### 4. PRESSURE SPIKE RESOLUTION AND FRICTION

The speed of modern EHL codes and the computers they are run on makes it possible to obtain solutions to line contact problems with up to  $10^6$  mesh points, as will be shown below. The quality of the results obtained varies between grid levels. This variation may give a larger error in key quantities of interest such as the total friction defined by Equation (10) than just discretisation error in quantities such as pressure or film thickness. For example the error in the total friction as defined by Equation (10) depends on errors in the reciprocal of film thickness and also on the pressure derivative  $\frac{\partial P}{\partial X}$ . As film thickness depends on all the pressures the error in the film thickness at any point depends on all the errors in the pressure values.

An example of this is shown in Figure 1 where the pressure distribution across the whole domain is shown. The non-dimensional parameters representing the input conditions of this simulation are shown

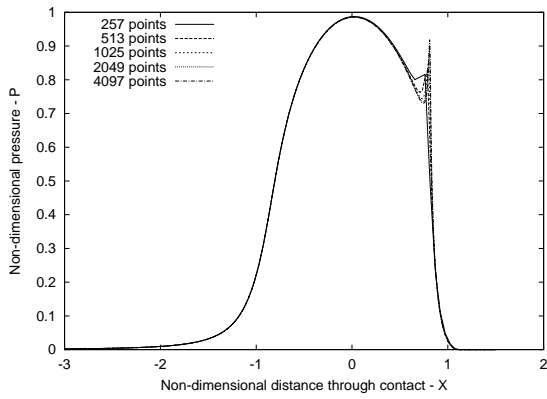


Figure 1. Non-dimensional pressure plot of a line contact problem with increasing mesh resolution

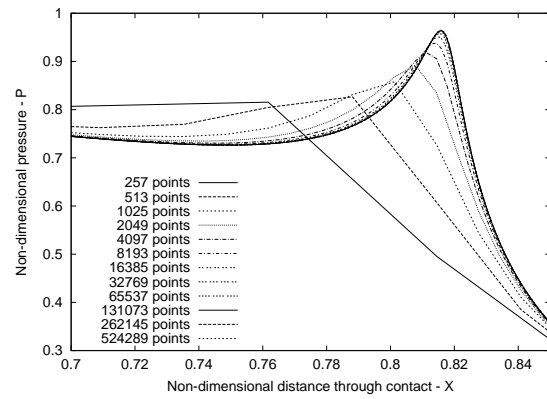


Figure 2. Non-dimensional pressure plot around spike with increasing mesh resolution

| Non-dimensional parameter | Value                  |
|---------------------------|------------------------|
| Moes M                    | 10.7                   |
| Moes L                    | 15.3                   |
| Material G                | $1.07 \times 10^{-10}$ |
| Speed U                   | $4.00 \times 10^3$     |
| Loading W                 | $1.57 \times 10^{-4}$  |

Table 1

Non-dimensional parameters for test case considered

in Table 1. It can be seen that the curves are almost coincidental apart from around the pressure spike. This area is shown in detail in Figure 2 where the addition of several orders of magnitude more points has now captured the pressure spike completely and appears to have achieved a converged continuous solution. Whilst on a nano-scale this profile could be considered as not representing the true behaviour of the contact it does, however, represent the true solution to the equations being solved numerically.

The effect of extra grids can be seen to only affect a small portion of the pressure plot, namely the spike area, and only to a very small degree once the grids greater than 4097 points have been reached. However as Figure 3 illustrates, the effect of the finer meshes on the spike has a more global effect on the film thickness. Similarly if we consider the total friction through the contact, as shown in Figure 4, the resolution of the spike is important if the total friction through the contact is to be calculated accurately.

In developing optimisation solvers for fitting model parameters to experimental results, see [9], the accu-

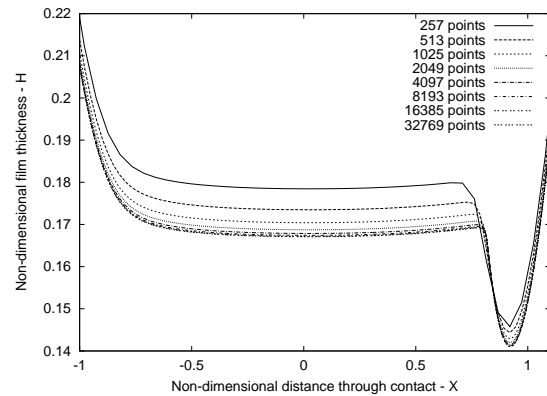


Figure 3. Non-dimensional film thickness plot of a line contact problem with increasing mesh resolution

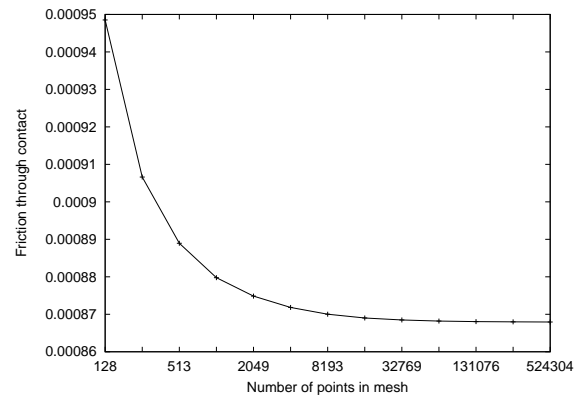


Figure 4. Total friction through the contact calculated with increasing mesh resolution

Parameters movable by optimiser:

| Variable       | Description                                            |
|----------------|--------------------------------------------------------|
| $\beta$        | Temperature coefficient of viscosity ( $K^{-1}$ )      |
| $z_0$          | Viscosity parameter                                    |
| $z_1$          | Viscosity parameter                                    |
| $K_0$          | Inverse critical shear rate (s)                        |
| $\bar{\alpha}$ | Pressure coefficient of inverse critical shear rate    |
| $\bar{\beta}$  | Temperature coefficient of inverse critical shear rate |
| $\bar{z}_0$    | Inverse critical shear rate parameter                  |
| $\bar{z}_1$    | Inverse critical shear rate parameter                  |
| $m$            | Cross exponent                                         |
| $a$            | Carreau-Yusada parameter                               |

Supplied physical conditions

| Cases                       | Condition                |
|-----------------------------|--------------------------|
| Cases 1-18                  | Ambient temperature 373K |
| Cases 19-36                 | Ambient temperature 313K |
| Cases 1-6, 19-24            | Load $4.30 \times 10^8$  |
| Cases 7-12, 25-30           | Load $5.66 \times 10^8$  |
| Cases 13-18, 31-36          | Load $6.73 \times 10^8$  |
| Cases 1, 7, 13, 19, 25, 31  | Slide to roll ratio 0.1  |
| Cases 2, 8, 14, 20, 26, 32  | Slide to roll ratio 0.2  |
| Cases 3, 9, 15, 21, 27, 33  | Slide to roll ratio 0.4  |
| Cases 4, 10, 16, 22, 28, 34 | Slide to roll ratio 0.7  |
| Cases 5, 11, 17, 23, 29, 35 | Slide to roll ratio 1.0  |
| Cases 6, 12, 18, 24, 30, 36 | Slide to roll ratio 1.4  |

Table 2

Variables and fixed quantities in the EHL optimiser

ray of the calculated values of the total friction is very important. In this work many thousands of EHL solutions are performed in order to optimise lubricant parameters for numerical friction calculations being compared against measured total friction through an experimental test rig. These experiments have been performed at a variety of different loadings, ambient temperatures and slide to roll ratios. These different sets of parameters are outlined in Table 2, along with the ranges of the supplied known conditions. By successive calls to a EHL solver cycling through these known physical conditions it is possible to vary the lubricant parameters to find the best set for matching the friction.

In a solver such as this it is important to understand the error in the numerical solution. In Figure 5 we show the percentage error in the key variables for each of 36 cases (two ambient temperatures, three loadings and six slide to roll ratios) with one input set of lubricant parameters for various different levels of grid, when compared against a very fine grid case. What the results show us is that for the standard quantities normally considered to be important (minimum and central film thicknesses and  $H_{00}$ ) the behaviour of the error between grids seems independent of case, especially for the more realistic thermal cases. In the case of friction however this relationship does not seem to hold. There is a strong correlation between errors in central and minimum film thickness, as shown in the correlation diagram of Figure 6. The overall measures of correlation of the four key variables are given in Ta-

| Variables compared    | Correlation, $\mathcal{C}$ |
|-----------------------|----------------------------|
| Friction - $H_{00}$   | 0.45                       |
| Friction - $H_{min}$  | 0.75                       |
| Friction - $H_{cen}$  | 0.78                       |
| $H_{00}$ - $H_{min}$  | 0.54                       |
| $H_{00}$ - $H_{cen}$  | 0.60                       |
| $H_{min}$ - $H_{cen}$ | 0.96                       |

Table 3

Correlation coefficients between errors in key variables for the thermal cases

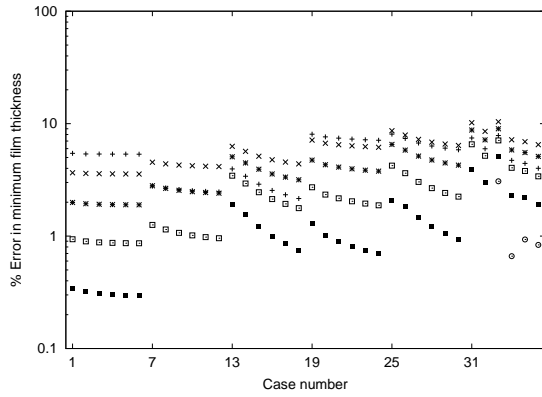
ble 3 where the correlation,  $\mathcal{C}$ , between quantities  $A$  and  $B$  is defined to be

$$\mathcal{C}(A, B) = \frac{\mu_{11}^2}{\sigma_A \sigma_B} \quad (11)$$

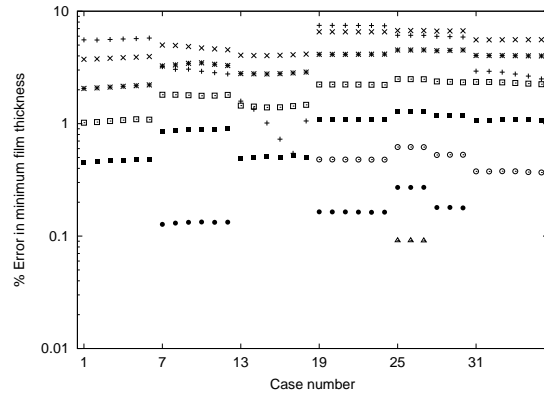
for variances  $\sigma_A$  and  $\sigma_B$  with covariance  $\mu_{11}$ , as in standard mathematical statistics, e.g. [14]. Given that we are expecting all the accuracies to improve with increased mesh resolution then any correlations below 0.9 show little dependence.

The left half of Figure 5, cases 1 to 18, has the lower ambient temperature, and these results are significantly better than those at the higher temperature. The results also seem to have better accuracy at higher slide to roll ratios and increasing loads.

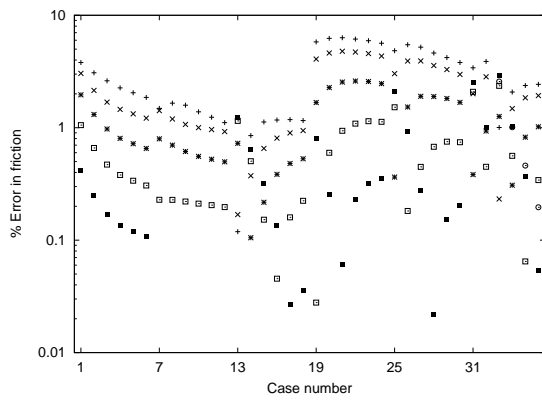
It is the derivatives of pressure in Equation (10) that are especially important in friction calculations. If the pressure spike is not captured well enough then these derivatives will not represent the true friction through



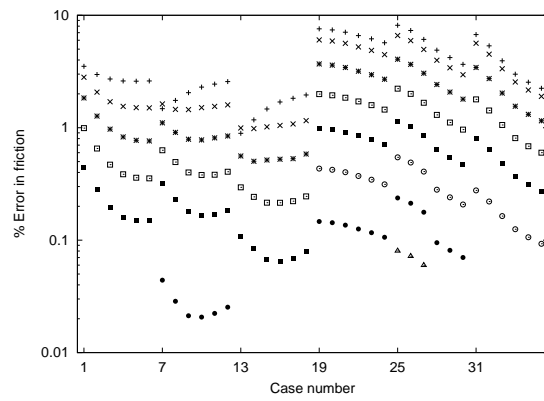
(a) Minimum film thickness - isothermal



(c) Minimum film thickness - thermal



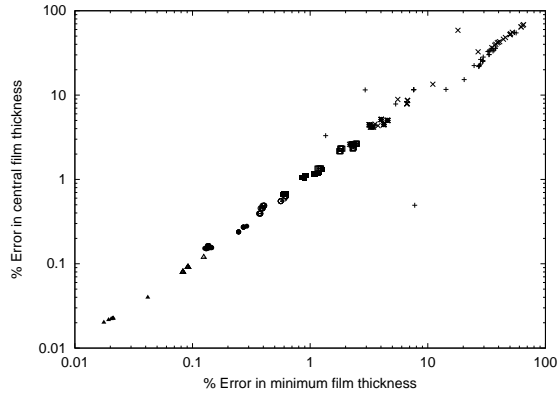
(b) Total friction - isothermal



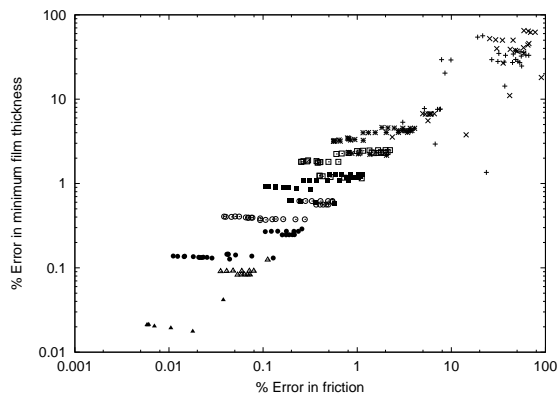
(d) Total friction - thermal

Key: + 257 points   \* 1025 points   ■ 4097 points   • 16385 points  
 × 513 points   □ 2049 points   ⊙ 8193 points   △ 32769 points

Figure 5. Percentage error in key variables against a truth mesh for both thermal and isothermal cases, with increasing grid accuracy having lower errors



(a) Minimum vs central film thickness errors



(a) Friction vs minimum film thickness errors

Figure 6. Correlation between percentage errors in (a) central and minimum film thicknesses, and (b) friction and minimum film thickness on increasingly fine grids for thermal cases

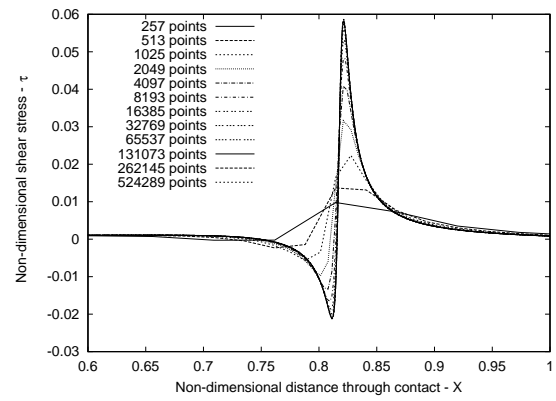


Figure 7. Shear stress profiles with increasing grid resolution for a line contact case

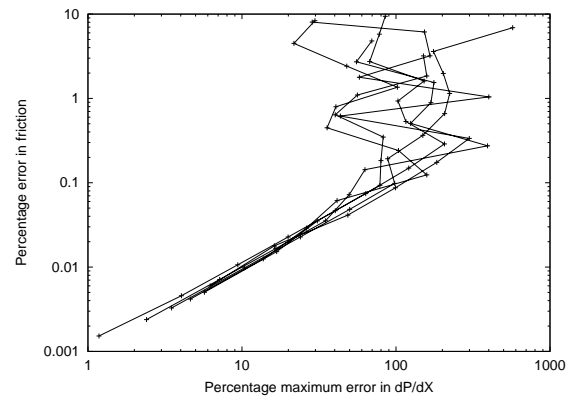


Figure 8. Correlation between the error in friction and the maximum error in the calculated values  $\frac{\partial P}{\partial X}$

the contact. These derivatives are also present through the calculation of the shear stress, as given in Equations (8,9). These shear stresses have an even more extreme profile on finer meshes as shown in Figure 7. It can be seen how the results on grid levels where the calculated key quantities have converged are still not capturing the maximum shear stress very accurately at all. The correlation between the error in maximum pressure derivative and friction shows that very fine grids are needed. This can be seen in Figure 8 where the increasing accuracy with which the pressure gradients are captured has a very strong correlation with the total friction errors through the contact. The fig-

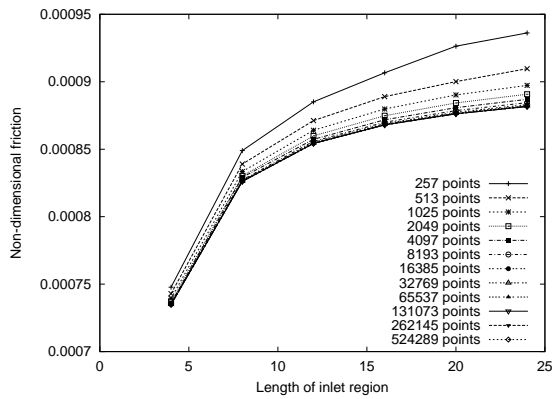


Figure 9. Calculated friction against length of inlet domain for increasing grid resolution in a line contact case

ure also shows that when the percentage error in the pressure derivative is large the error in friction is uncertain.

The size of the domain used for the calculation of friction is also very important. In Figure 9 we show the calculated friction against the length of the negative  $X$  domain, i.e.  $-X_l$  for fixed grid levels. It is seen that with very large negative domains, i.e. large inlet regions, the friction converges to a particular value. Obviously for each grid level the mesh spacing will increase as the value of  $X_l$  gets larger, however it can be seen that this is not enough to account for the convergence behaviour of the friction. The conclusion to be drawn is that the inlet region has a very important effect on the friction results calculated, in many cases over 10% of the calculated friction.

## 5. GRID ADAPTATION

The previous sections have shown that whilst the pressure spike requires a very fine mesh in order to fully resolve it, there appears very little change in the rest of the pressure solution after 4097 points have been used. Consequently a solution to the problem of correctly resolving the spike without resorting to meshing the domain with a fine mesh is to use grid adaptation. EHL work on adaptation within the multigrid scheme was initially considered by Lubrecht [16] and later by Goodyer *et al.* [8,11,10]. In the latter works, which are mainly for point contact cases, re-

sults show substantial computational time savings are possible by restricting the fine mesh to the contact region and even smaller regions therein. The adaptation criteria could be based on measurable quantities from the solution, such as the gradients of the calculated pressure profile. A more automatic method used in both [8] and [16] is that of Bai and Brandt [1]. This uses the relative truncation error between grids as a measure of the extent to which the local introduction of the finer grid has influenced the global solution [19]. In this work we have not employed the  $\lambda$ -FMG algorithm described in [1], which is optimal with regards to the amount of work per multigrid cycle, but a regular FMG algorithm with a predefined finest grid, such as described in [19].

The mesh adaptation strategies we have employed add extra grid levels into the multigrid scheme only when suggested by the mesh refinement algorithm, based on local mesh refinement. The solution values at points on the boundaries of these regions are treated as Dirichlet values and taken as fixed from the coarser level. However, the work effort of the entire multigrid cycle is now no longer optimal [1]. The linear algebra systems used in what had been a line scheme are now reduced from length  $N_X$  to just the length of each adapted region. In practice this will lead to significant reductions in computation time.

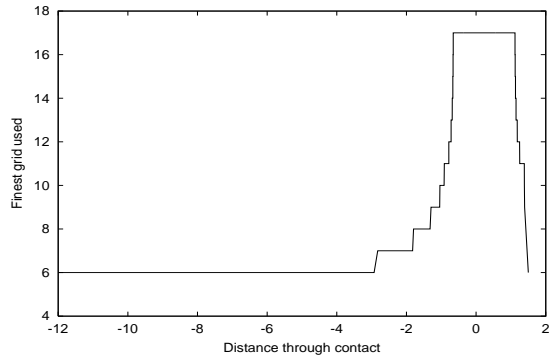
Since the cavitation boundary must be allowed to move in the positive as well as the negative  $X$ -directions there needs to be two points from the cavitation region included in the linear algebra line solve. This also implies the true free boundary condition of  $\frac{\partial P}{\partial X} = 0$  at the edge of the cavitation region.

Using the test case defined in Table 1 it is possible to draw some conclusions about the use of adaptation. The first issue concerns the most appropriate way in which to drive the areas of the mesh receiving extra adaptation. If very large domains are needed to accurately capture the total friction, as suggested from Figure 9, then clearly a fine mesh in this inlet region is highly undesirable.

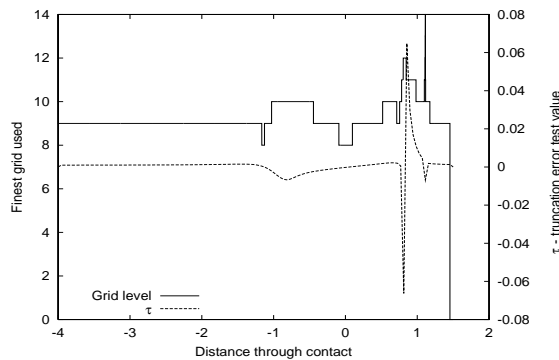
Examples of the line meshes we use are shown in Figure 10 with adaptation criteria being based on (a) pressure, and (b) the  $\tau_{k-1}^k$  test, [1]. The use of the safety layers around adapted regions is noticeable in both of these pictures along with how little of the grid needs the finest levels of resolution. Also shown in Figure 10(b) are the values of the truncation error on which the adaptation is based.

We have chosen to compare the accuracy of the





(a) Pressure solution based



(b) Truncation error

Figure 10. Example meshes used for adaptation: left hand axis shows finest grid level used

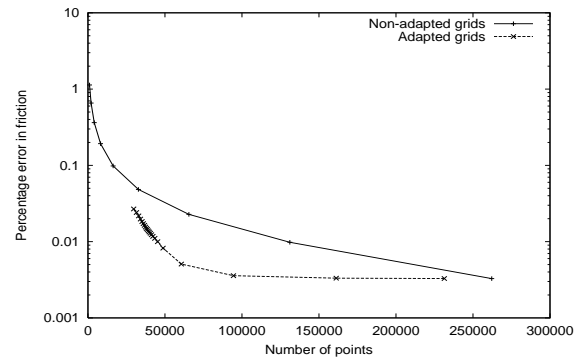


Figure 11. Percentage errors for adapted cases against number of points used

adaptation schemes in this work based on the friction since we have shown in the previous section how important this is. In Figure 11 we are using a truth mesh solution of 524289 points (grid 18) to compare the percentage errors for the calculated friction against the number of points used. The curves plotted are the errors without using any grid refinement at each level of coarser mesh and the curves for the meshes in Figure 10a. It is seen how the actual friction results are of the same order of accuracy, even with much lower numbers of fine grid points being used.

## 6. TRANSIENT CASES

All EHL cases are inherently transient. The numerical errors incurred at each timestep will grow and this local error must be maintained at no more than the discretisation error of the solution. Variable timestepping for EHL solutions was shown by Goodyer *et al.* [11,8] to be successful at accomplishing this, and gave significant savings in computational solution time.

In the previous section we have shown how improved resolution of the pressure derivative has enabled more accurate numerical solutions to steady state cases to be achieved. The same techniques extend into transient cases. Here we consider two different cases of applying surface roughness patterns to the contact. The first is a single asperity passing through the contact in a cyclic manner. The second is a full measured surface roughness profile.

The results for all transient cases are considered

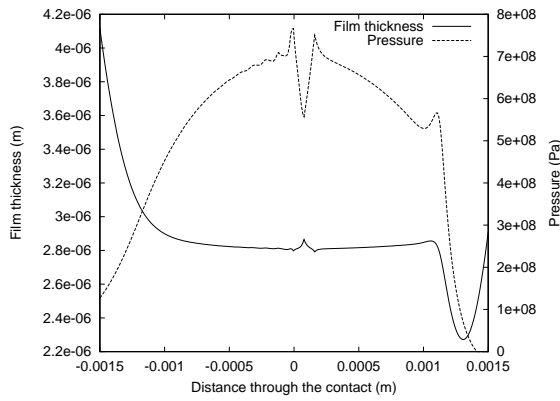


Figure 12. Pressure and film thickness at a typical moment of a single asperity passing through the contact area

starting from the steady state case. The adaptive multigrid algorithm described previously is applied on each timestep using V-cycles. Timestepping is fixed with  $\Delta X = \Delta T$  since it has previously been shown in [8] that variable timestepping is most effective when other aspects of the transient process are more important to the non-linear effects, such as changing surface speeds and loadings; overrolling of surface features tends to require a standard timestep when the asperity is in the contact region. The error based convergence tests applied on each timestep, presented for EHL cases in [11], are used to maximise the accuracy to work ratio.

In this section we are again considering the differences with increasing resolution of grids. The surface roughness profiles used have 256 data points spread along the domain. For finer grids the profile is linearly interpolated from this resolution.

Intuitively, the overrolling of a single asperity should be very similar to the steady state case, as presented in the previous sections, with the different initial frictions arising from the choice of mesh resolution being important. In Figure 12 at a typical moment of the asperity passing through the contact area the pressure and film thickness profiles are shown. It can be seen that in this case the asperity, and hence the change to the pressure solution, is not very large. However in Figure 13 we see the friction at grid resolutions increasing from the level of the fixed roughness profile. It is clear that the similar behaviour shown on the coarser grids is less marked on the finest grid where the transient effects from previ-

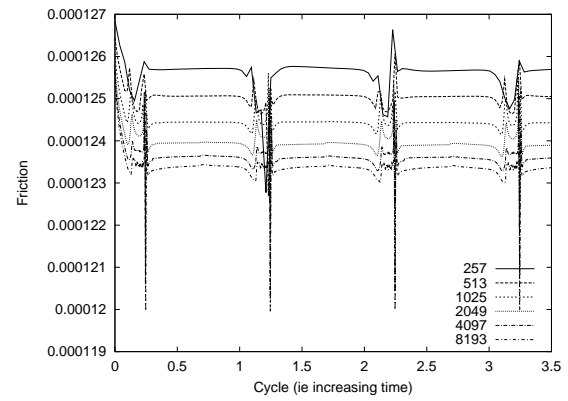


Figure 13. Friction against time for a single asperity passing through an EHL contact for increasing grid resolution. The time axis indicates the number of times the asperity has passed through

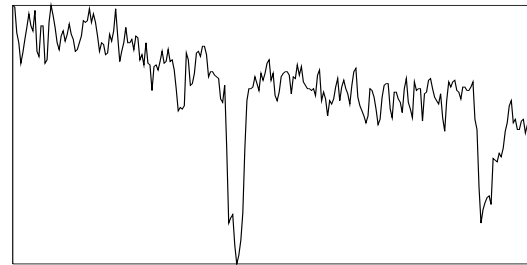


Figure 14. Measured surface roughness profile applied along the contact, average non-dimensional roughness  $1.6 \times 10^{-2}$

ous timesteps are seen to be very influential in damping the friction changes.

Finally we consider the case of applying the real surface roughness profile shown in Figure 14 to the contact. Here the contact is always having to resolve steep pressure gradients from the pressure, with the roughness amplitude limited to be of the same order as that in Figure 12. In this case only the first few timesteps are shown since the results continue in a similar manner, as would be expected.

The results for friction are shown in Figure 15. It can be seen that with extra grid resolution many more features are being picked out in the transient solution. The use of smaller timesteps obviously aids better accuracy, but the position of some of the features also appears to be resolved more accurately. This is prob-

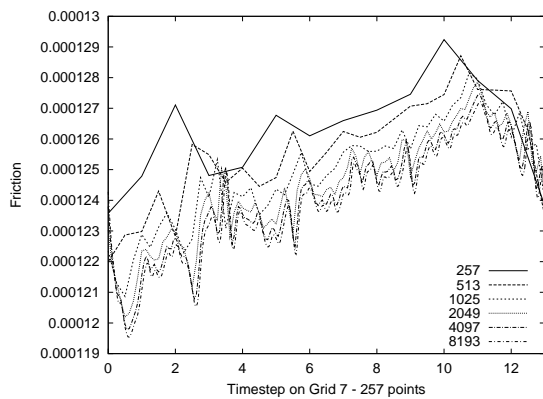


Figure 15. Transient results for friction in a real surface roughness contact with increasing grid resolution

ably due to the non-linear effects coming from the squeeze term being captured and resolved.

Results for friction for all the transient cases we have considered again highlight the importance of increased grid resolution. For the surface roughness cases shown, the more points that are used enables better resolution of all the micro-EHL problems and associated pressure gradients.

The benefit of the extra resolution provided by the finer meshes and smaller timestep is clearly seen in the convergence of the friction solutions shown in Figure 15. It is worth bearing in mind the extra effort required to get the solutions on the finer grids. The matching of spatial and temporal timesteps means that for the five extra grid resolutions, i.e. 32 times as many points being used, then we require 32 times as many timesteps. When combined with the expense of each single calculation, even using MLMI, this is a serious extra cost. Once again this highlights the need to use adaptive techniques in the solver. The roughness profile used here could have been applied over a shorter length and hence even more points would have been necessary to resolve the solution at each timestep.

## 7. CONCLUSIONS AND FUTURE WORK

In this paper we have considered how to get the most computationally efficient solutions for the problems considered. It has been seen how the extra resolution of very fine grids has enabled features associated with the pressure spike to be accurately resolved. The consideration of global quantities, such as the to-

tal friction through the contact, has been seen to be very much influenced by how accurately this pressure spike is captured.

Grid adaptation for EHL cases, which has been shown in previous work, has been seen to be efficient in achieving line contact solutions with very high accuracy. The use of both predetermined adapted regions and a truncation error test has been seen to be very efficient in selecting the regions to be adapted for accuracy of the total friction. It has been seen how an accurate calculated total friction has been achieved with far fewer points, and hence computational expense, than by using the fine mesh everywhere.

When used in transient cases, grid adaptation gives equally good improvements in solution quality as for steady state cases. Inclusion of the transient derivatives in areas where the total solution is changing little between timesteps suggests there will be less need for fine resolution in these parts of the computational domain. Extra grid resolution has been shown to refine and resolve features not noticeable on coarser grids. The growth of global errors has also been seen to be minimised.

Extending these methods to point contact cases is theoretically not a problem. The issues are now more concerned with how well the solution can be represented. The pressure spike from the line contact case becomes a pressure ridge, and for the equivalent number of points to capture the gradients then much larger meshes than have been considered for EHL problems will be necessary. Parallel computing techniques, such as shown in [12] have enabled point contact solutions of up to 67 million points, for real roughness cases but it has been shown here how this resolution will not always be good enough. Point contact cases with real surface roughness will obviously have many more pressure gradients requiring refinement and hence calculations for the total friction will be very demanding.

## REFERENCES

1. D. Bai and A. Brandt. Local mesh refinement multigrid techniques. *SIAM Journal on Scientific and Statistical Computing*, 8(2):109–134, 1987.
2. E. J. Bissett and D. W. Glander. A highly accurate approach that resolves the pressure spike of elastohydrodynamic lubrication. *Journal of Tribology*, 110:241–246, 1988.
3. P. J. Blau. *Friction Science and Technology*.

- Dekker, 1996.
4. K. A. Blencoe, G. W. Roper, and J. A. Williams. The influence of lubricant rheology and surface topography in modelling friction at concentrated contacts. *Proceedings of the Institution of Mechanical Engineers Part J, Journal of Engineering Tribology*, 212(6):391–400, 1998.
  5. A. Brandt and A. A. Lubrecht. Multilevel matrix multiplication and fast solution of integral equations. *Journal of Computational Physics*, 90(2):348–370, 1990.
  6. D. Dowson and G. R. Higginson. *Elastohydrodynamic Lubrication, The Fundamentals of Roller and Gear Lubrication*. Pergamon Press, Oxford, Great Britain, 1966.
  7. R. Fairlie, C. E. Goodyer, M. Berzins, and L. E. Scales. Numerical modelling of thermal effects in elastohydrodynamic lubrication solvers. In D. Dowson *et al.*, editor, *Tribological Research and Design for Engineering Systems, Proceedings of the 29<sup>th</sup> Leeds-Lyon Symposium on Tribology*, pages 675–683. Elsevier, 2003.
  8. C. E. Goodyer. *Adaptive Numerical Methods for Elastohydrodynamic Lubrication*. PhD thesis, University of Leeds, Leeds, England, 2001.
  9. C. E. Goodyer, M. Berzins, P. K. Jimack, and L. E. Scales. Grid-based numerical optimisation in a problem solving environment. In S. Cox, editor, *Proceedings of the All Hands Meeting 2003*, pages 854–861. EPSRC, 2003. ISBN: 1-904425-11-9.
  10. C. E. Goodyer, R. Fairlie, M. Berzins, and L. E. Scales. Adaptive mesh methods for elastohydrodynamic lubrication. In *ECCOMAS CFD 2001 : Computational Fluid Dynamics Conference Proceedings*. Institute of Mathematics and its Applications, 2001. ISBN: 0-905-091-12-4.
  11. C. E. Goodyer, R. Fairlie, M. Berzins, and L. E. Scales. Adaptive techniques for elastohydrodynamic lubrication solvers. In G. Dalmaz *et al.*, editor, *Tribology Research: From Model Experiment to Industrial Problem, Proceedings of the 27<sup>th</sup> Leeds-Lyon Symposium on Tribology*, pages 709–719. Elsevier, 2001.
  12. C. E. Goodyer, J. Wood, and M. Berzins. A parallel Grid based PSE for EHL problems. In J. Fagerholm, J. Haataja, J. Järvinen, M. Lyly, Rback P., and V. Savolainen, editors, *Applied Parallel Computing, Proceedings of PARA '02, Lecture Notes in Computer Science*, volume 2367, pages 523–532. Springer, 2002.
  13. R. W. Hall. Pressure spikes in elastohydrodynamics - some elastic considerations. *WEAR*, 131(1):151–161, 1988.
  14. P. G. Hoel. *Introduction to Mathematical Statistics*. Wiley, 1984.
  15. R.-T. Lee and C.-H. Hsu. A fast method for the analysis of thermal-elastohydrodynamic lubrication of rolling/sliding line contacts. *WEAR*, 166(1):107–117, 1993.
  16. A. A. Lubrecht. *Numerical solution of the EHL line and point contact problem using multigrid techniques*. PhD thesis, University of Twente, Enschede, The Netherlands, 1987. ISBN 90-9001583-3.
  17. C. J. A. Roelands. *Correlational Aspects of the viscosity-temperature-pressure relationship of lubricating oils*. PhD thesis, Technische Hogeschool Delft, The Netherlands, 1966.
  18. L. E. Scales. Quantifying the rheological basis of traction fluid performance. In *Proceedings of the SAE International Fuels and Lubricants Meeting, Toronto, Canada*. Society of Automotive Engineers, 1999.
  19. U. Trottenberg, C. Oosterlee, and A. Schüller. *Multigrid*. Academic Press, 2001.
  20. C. H. Venner. *Multilevel Solution of the EHL Line and Point Contact Problems*. PhD thesis, University of Twente, Enschede, The Netherlands, 1991. ISBN 90-9003974-0.
  21. C. H. Venner and A. A. Lubrecht. *Multilevel Methods in Lubrication*. Elsevier, 2000.
  22. M. F. Workel, D. Dowson, P. Ehret, and C. M. Taylor. The influence of mean contact pressure on the friction coefficient of a traction fluid at high pressure. *Proceedings of the Institute of Mechanical Engineers Part C, Journal of Mechanical Engineering Science*, 214:309–312, 2000.